S. E. Bechtel
D. B. Bogy
F. E. Talke

Impact of a Liquid Drop Against a Flat Surface

Lagrangian methods are used with an assumed flow field and a truncated sphere model to analyze the dynamical process of a liquid drop impacting a flat, rigid surface. The resulting differential equation for drop height as a function of time during contact is solved numerically for several values of the three parameters: Weber number of the incoming drop, ratio of the surface tension in air to that at the contact surface, and the viscosity parameter. The drop contact radius as a function of time is also calculated and compared with some experimental results in the literature.

Introduction

Liquid drop impact with a solid surface has been a topic of interest in many different engineering applications. At present the main interests are in connection with nuclear reactor cooling and ink-jet printing. In the former application heat transfer is affected by the drop dynamics upon impact of the drop with a hot surface. In the latter the eventual spot size produced is affected by the drop dynamics upon impact with the paper. Our concern is with ink drop spot size.

We can separate the process of producing an ink spot into two distinct parts. First is the drop shape resulting from the dynamics of impact. Second is the final spot size after penetration of the liquid into the paper and subsequent drying. The latter part has been considered by Cantow and Nebenzahl [1]. Here we are concerned with the impact dynamics, and we assume that the dynamical process is completed before the penetration is begun. We therefore idealize the dynamical process by assuming that the target surface is flat, rigid, and impenetrable.

Early studies of drop impact were concerned with cavitation damage on steam turbine blades and later with rain damage on aircraft surfaces. Engel [2] presents high speed photographs and schlieren patterns of water drops impacting a glass surface. These photographs show the spherical drop initially deforming to a shape similar to a truncated sphere and later spreading to a circular disk shape. No recovery and bounce-off phenomenon was indicated from these experiments. An energy balance type analysis was used to predict the impact pressure as a function of time.

Wachters and Westerling [3] presented experimental results for drop impact on a 400°C polished gold surface. Since vaporization occurs between the drop and the surface, wetting does not occur and the drops bounce away after a period of near contact during which there is a flattening and then a recovery of the drop. They observed that the drops tend to splatter if the Weber number $W = \rho a U^2/\sigma$ is greater than 80, where ρ and σ are fluid density and surface tension, respectively, a is the drop diameter, and U is the drop velocity. Similar observations were made by Pederson [4] and by Styricovich *et al.* [5].

A recent study by Kendall and Rohsenow [6] was concerned with heat transfer to dispersed flows and sprays. They showed that low heat transfer rates are associated with the rebounding of drops after impact from very hot surfaces. They developed an analytical model of the drop impact dynamics based on Lagrangian methods. Two drop models—cylindrical and truncated sphere—were considered. Drop height and radius were calculated based on the cylindrical model. These results were compared with experiments and were found to be in reasonable agreement.

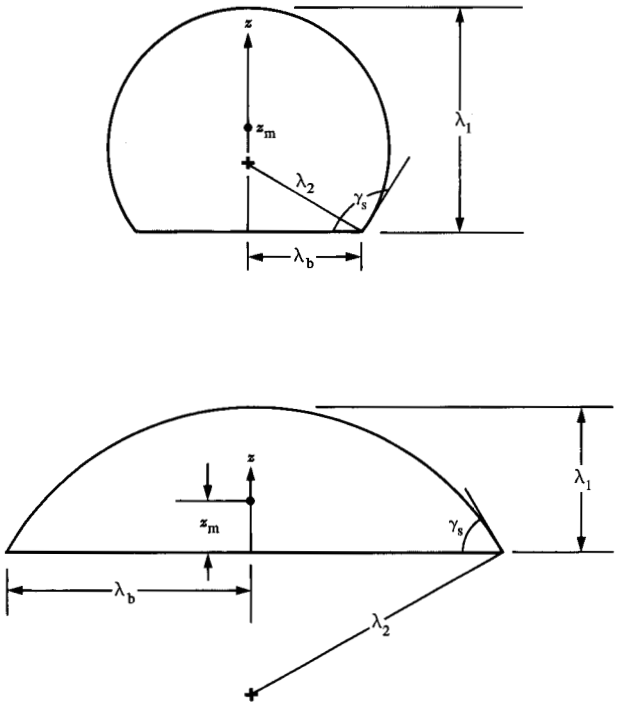

Figure 1 Truncated sphere geometries.

Our analysis is similar to that of [6]. We use a truncated sphere model with Lagrangian methods and an assumed flow field. Our approach differs from that in [6] in that we use a different expression for kinetic energy, we include different surface tension values for the free surface and contact surface of the drop, and we include viscous dissipation. A second order nonlinear, ordinary differential equation is derived for determining the drop height as a function of time during contact. This equation is solved numerically for various values of the Weber number, surface tensions, and viscosity. Drop contact radius is also calculated, and the results are compared with some experimental results in the literature.

Problem formulation

Assume that a spherical liquid drop of diameter a, density ρ, and free surface tension σ (in air) impacts a flat rigid stationary target surface with velocity U. We neglect the interaction between the drop and air, and we let σ_b denote the interface tension between the drop and target surface.

Rather than attempt to solve this flow problem by use of the continuum theory of fluid mechanics, we use a dynamical model based on Lagrangian methods together with certain assumptions about the drop deformation. In a manner similar to that used by Kendall and Rohsenow [6] we assume the drop is of constant volume and, after contact with the target surface, has the shape of a truncated sphere. Figure 1 shows two configurations of such a truncated sphere in contact with the target surface, which is located at $z = 0$. The geometry of the truncated sphere can be expressed in terms of the height λ_1, which gives the maximum distance on the drop surface from the target surface. If the drop is not in contact with the target surface, an additional parameter, say the location of the mass center z_m, is required to specify the geometry. It will be convenient in deriving the equation that determines λ_1 as a function of time during contact to use both parameters λ_1 and z_m. The relationship between them supplies a measure of the drop deformation.

Let λ_2 and λ_b denote the spherical radius and the contact circle radius of the truncated sphere. Defining the dimensionless drop height x by

$$x = \lambda_1/a, \tag{1}$$

we obtain from the geometry of the truncated sphere the results

$$\lambda_2/a = x(2 + x^{-3})/6, \lambda_b/a = [(x^{-1} - x^2)/3]^{1/2} = N(x). \tag{2}$$

By use of the definition of mass center and after performing the required volume integrations, we obtain the following relationship between z_m and λ_1 during contact:

$$z_m/a = (2x + x^4)/6 = M(x). \tag{3}$$

The drop volume V, free surface area A, and contact surface area A_b are given by

$$V = \pi a^3/6, A = 2\pi\lambda_1\lambda_2, A_b = \pi(2\lambda_1\lambda_2 - \lambda_1^2). \tag{4}$$

Initially, when the spherical drop first touches the target surface, the parameters defined above have the values

$$\lambda_1^0 = a, \lambda_2^0 = a/2, \lambda_b^0 = 0, z_m^0 = a/2$$
$$A^0 = \pi a^2, A_b^0 = 0. \tag{5}$$

The potential energy of the drop due to surface and interface tension is given by

$$\begin{aligned} PE &= \sigma A + \sigma_b A_b \\ &= (\sigma a^2\pi/3)\{2x^2 + x^{-1} + (\sigma_b/\sigma)[x^{-1} - x^2]\} \\ &= \sigma a^2 L(x). \end{aligned} \tag{6}$$

The kinetic energy is given by

$$KE = \frac{1}{2}\rho \int_V (U_r^2 + U_z^2)\, dV, \tag{7}$$

where U_r and U_z represent the radial and axial compo-

nents of the flow velocity. In order to express KE in terms of dx/dt we must have a particular form for the velocity field. For this we assume the axisymmetric stagnation point flow for inviscid irrotational conditions (see Batchelor [7]), which can be written in the form

$$U_r = -\frac{1}{2}\frac{M'(x)}{M(x)}\frac{dx}{dt}r,$$

$$U_z = \frac{dz_m}{dt} + \frac{M'(x)}{M(x)}\frac{dx}{dt}(z - z_m). \tag{8}$$

This axisymmetric velocity field clearly satisfies

$$\frac{1}{r}\frac{\partial(rU_r)}{\partial r} + \frac{\partial U_z}{\partial_z} = 0, \frac{\partial U_r}{\partial z} - \frac{\partial U_z}{\partial r} = 0. \tag{9}$$

It also has a stagnation point at the origin and satisfies the inviscid boundary condition at $z = 0$, since from (8) and (3) it follows that

$$U_r(0, 0, t) = 0, U_z(0, 0, t) = 0, U_z(r, 0, t) = 0. \tag{10}$$

Finally, it includes a specific measure of the drop deformation by relating the flow field to the mass center. With use of (8) and (3) in (7) we obtain, after integrating over the volume of the truncated sphere,

$$KE = \frac{1}{2}\rho\left[\frac{M'(x)}{M(x)}\frac{dx}{dt}\right]^2\int_V (z^2 + r^2/4)\,dV$$

$$= \rho V a^2 A(x)\left(\frac{dx}{dt}\right)^2, \tag{11}$$

in which

$$A(x) = \left[\frac{M'(x)}{M(x)}\right]^2\left(\frac{13x^5}{180} + \frac{11x^2}{144} + \frac{x^{-1}}{72}\right). \tag{12}$$

We observe that the initial values of PE and KE are given by

$$PE^0 = \sigma\pi a^2, KE^0 = \pi a^3\rho U^2/12. \tag{13}$$

The initial Weber number, defined by

$$W = \rho a U^2/\sigma, \tag{14}$$

can be expressed also as

$$W = 12\,KE^0/PE^0. \tag{15}$$

It is found experimentally (see [3]) that drop splatter occurs for $W > 80$ so our analysis will be restricted to initial Weber numbers below this value.

Derivation of the differential equation for the drop height

We begin with the variational statement

$$\int_{t_1}^{t_2}\left[\delta(KE - PE) - \int_{A_b}\tau\delta d_r\,dA\right]dt = 0, \tag{16}$$

in which τ represents a shear stress and d_r is the radial displacement on the contact surface of the drop. Since no shear stress is developed by the velocity field (8), we make the assumption that the shear stress at $z = 0$ is proportional to U_r, *i.e.*,

$$\tau = C\mu U_r, \tag{17}$$

in which μ is the fluid viscosity and C is a constant with the dimension of inverse length. The radial displacement d_r associated with U_r in (8) is given by

$$d_r = -\frac{1}{2}\ln[M(x)]r. \tag{18}$$

Using (6), (8), (11), (12), (17), and (18) in (16), and carrying out the variations with x as the independent parameter assumed to vanish at t_1 and t_2, we obtain the nonlinear, second order differential equation

$$2A(x)\frac{d^2x}{dt^2} + A'(x)\left(\frac{dx}{dt}\right)^2 + \frac{\mu C}{12\rho a}B(x)\frac{dx}{dt}$$

$$+ \frac{\sigma}{\rho V}L'(x) = 0 \tag{19}$$

subject to the initial conditions

$$x(0) = 1, \left.\frac{dx}{dt}\right|_{t=0} = -U/a. \tag{20}$$

In (19) the function $A(x)$ describes the kinetic energy given in (11), $L'(x)$ describes the derivative of the potential energy in (6), $M(x)$ relates the drop height to the mass center in (3), while $B(x)$ derives from the dissipation term in (16) and is given by

$$B(x) = [M'(x)/M(x)]^2(x^4 - 2x + x^{-2}). \tag{21}$$

It is convenient to introduce dimensionless time t^* and surface tension and viscosity parameters ST and VIS, respectively, through

$$t^* = t/\left(\frac{\rho a^3}{\sigma}\right)^{1/2}, ST = \sigma_b/\sigma, VIS = \frac{aC}{12}\frac{W^{1/2}}{R}, \tag{22}$$

where R is a Reynolds number $R = \rho a U/\mu$. We also reduce the second order differential equation (19) to a first order system to obtain in dimensionless form

$$\dot{x} = y, \tag{23}$$

$$\dot{y} = -[C(x)y^2 + D(x)y + E(x)]/2A(x),$$

in which a dot denotes differentiation with respect to t^* and $C(x)$, $D(x)$, and $E(x)$ are defined by

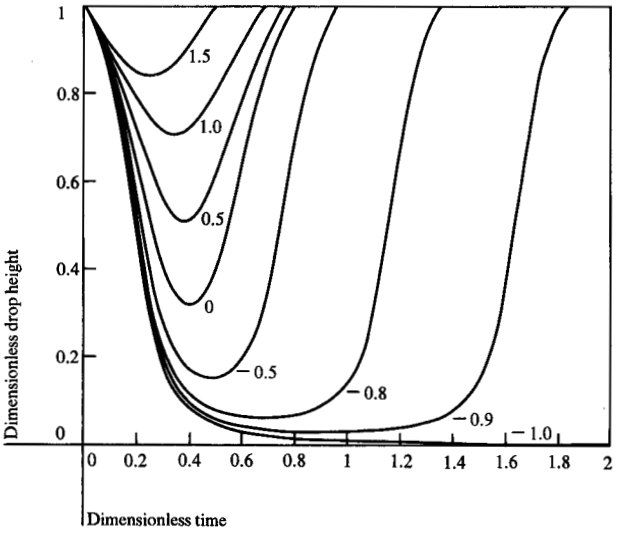

Figure 2 Drop height *vs* time during contact (for various *ST* with $W = 1$ and $VIS = 0$).

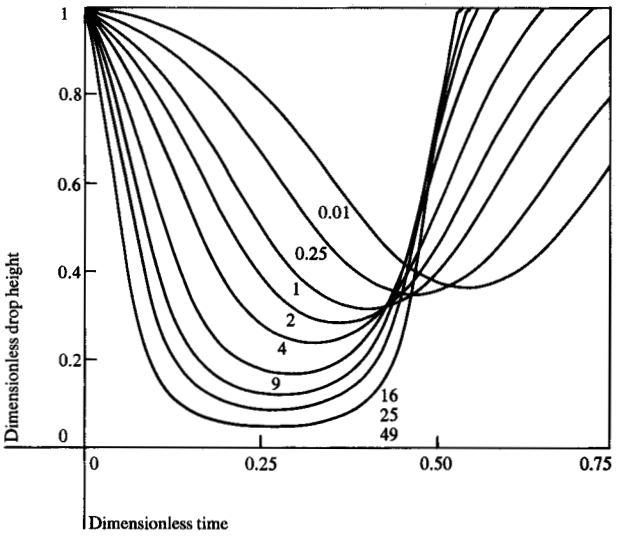

Figure 3 Drop height *vs* time during contact (for various *W* with $ST = 0$ and $VIS = 0$).

$$C(x) = \left(\frac{13x^4}{36} + \frac{11x}{72} + \frac{x^{-2}}{72}\right)\left(\frac{1}{3} + \frac{2x^3}{3}\right)^2\left(\frac{x}{3} + \frac{x^4}{6}\right)^{-2} + \left(\frac{13x^5}{90} + \frac{11x^2}{72} + \frac{x^{-1}}{36}\right)\left(\frac{1}{3} + \frac{2x^3}{3}\right) \cdot \left[2x^2\left(\frac{x}{3} + \frac{x^4}{6}\right) - \left(\frac{1}{3} + \frac{2x^3}{3}\right)^2\right] \cdot \left(\frac{x}{3} + \frac{x^4}{6}\right)^{-3}, \quad (24)$$

$$D(x) = VIS(x^4 - 2x + x^{-2})\left(\frac{1}{3} + \frac{2x^3}{3}\right)^2\left(\frac{x}{3} + \frac{x^4}{6}\right)^{-2},$$

$$E(x) = 2\,[4x - x^{-2} - ST(2x + x^{-2})].$$

The initial conditions for the system (23) are

$$x(0) = 1,\ y(0) = -W^{1/2}. \quad (25)$$

Numerical results

The differential system (23)–(25) was solved numerically by use of a Runge-Kutta method for several values of the parameters *W*, *ST*, and *VIS*. The parameter *W*, defined in (14), is a measure of the impact velocity. The parameter *ST* is the ratio of the surface tensions on the contact surface and free surface. The equilibrium shape of the drop, if it remains on the surface, is expressible in terms of this parameter, since from (19) the equilibrium drop height, $\bar{x}$, is given by

$$L'(\bar{x}) = 0, \quad (26)$$

which, from (6), implies

$$\bar{x} = [(1 + ST)/2(2 - ST)]^{1/3}. \quad (27)$$

This drop height is in agreement with that given by a truncated sphere with a static meniscus contact angle γ_s (see Fig. 1) related to *ST* by

$$\cos \gamma_s = -ST. \quad (28)$$

The parameter *VIS* is defined in (22) in terms of *W*, *R*, and an unknown constant *C* that introduces an effect similar to a boundary layer. We have not tried to determine a value for this constant. The inviscid case is represented by $C = 0$. In the numerical computations we merely chose values of *VIS* to observe the effect of viscosity.

Figure 2 shows the dimensionless drop height *x* as a function of dimensionless time t^* for the inviscid case, $VIS = 0$, and initial Weber number, $W = 1$, for various surface tension ratios, *ST*, ranging from 1.5 to −1.0. Under static conditions the contact angle γ_s in (28) would be 180 degrees for $ST = 1$, 90 degrees for $ST = 0$, and 0 degrees for $ST = -1$. For $|ST| > 1$ there is no interpretation of *ST* in terms of corresponding static contact angles. Figure 2 indicates that after impact the drop height decreases to a minimum, then rebounds to the initial spherical shape with $x = 1$ and leaves the surface. This is true for $ST > -1$, but for $ST = -1$, for which the static contact angle is 0 degrees, the drop continues to spread and does not rebound. The minimum drop height is strongly dependent on *ST*.

Figure 3 shows *x vs* t^* for $ST = 0$, $VIS = 0$, and various values of *W* between 0.01 and 49. The curve for $W = 1$ corresponds to the curve for $ST = 0$ in Fig. 2. These

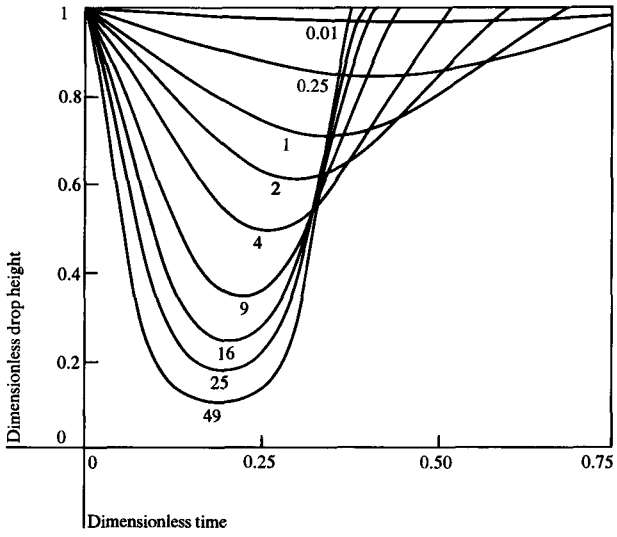

Figure 4 Drop height *vs* time during contact (for various W with $ST = 1$ and $VIS = 0$).

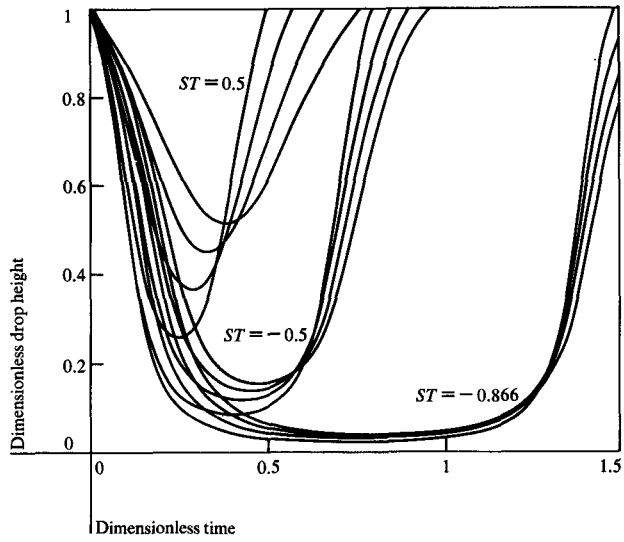

Figure 5 Drop height *vs* time during contact (for various ST with $W = 1, 2, 4, 9$ and $VIS = 0$).

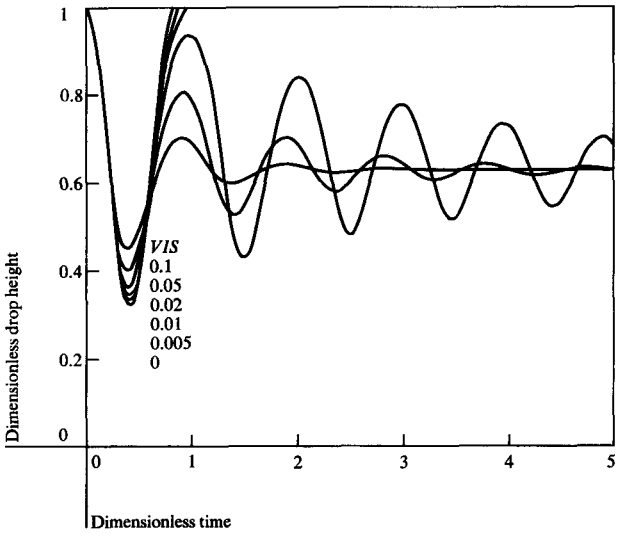

Figure 6 Drop height *vs* time during contact (for various *VIS* with $ST = 0$ and $W = 1$).

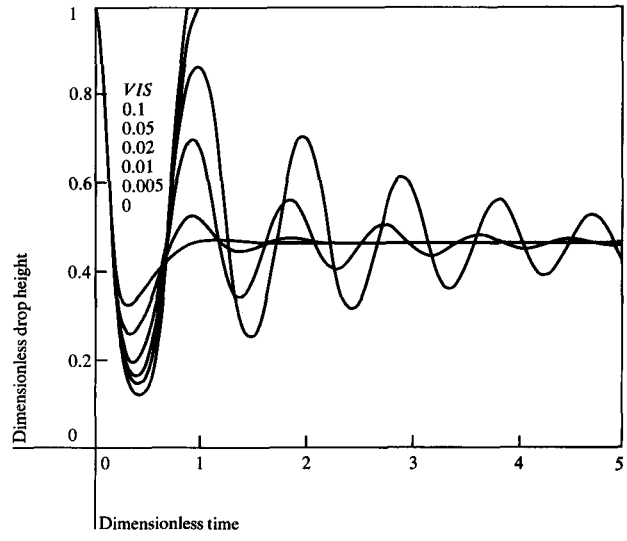

Figure 7 Drop height *vs* time during contact (for various *VIS* with $ST = -0.5$ and $W = 1$).

curves indicate the sensitivity of the minimum drop height to the impact velocity parameter W. They also show that the duration of contact is greater for smaller W. Figure 4 is similar to Fig. 3 except that $ST = 1$ rather than $ST = 0$. The curve for $W = 1$ corresponds to the curve for $ST = 1$ in Fig. 2.

Figure 5 also has $VIS = 0$ but shows x *vs* t^* for three values of ST and four values of W. The curves are similar to the other inviscid results in Figs. 2–4. Here we see that the dependence on ST is much stronger than the dependence on W for the ranges of these two parameters considered.

The numerical results in Figs. 6–14 illustrate the dependence of x *vs* t^* on the viscosity parameter *VIS*. Figures 6–8 have $ST = 0, -0.5, -0.866$, respectively, for $W = 1$; Figs. 9–11 have $ST = 0, -0.5, -0.866$, respectively, for $W = 4$; Figs. 12–14 have $ST = 0, -0.5, -0.866$, respectively, for $W = 49$. In each of these sets *VIS* ranges from

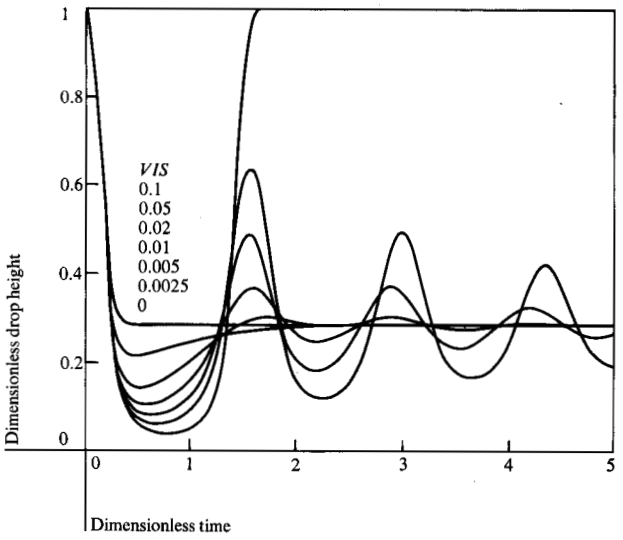

Figure 8 Drop height *vs* time during contact (for various *VIS* with $ST = -0.866$ and $W = 1$).

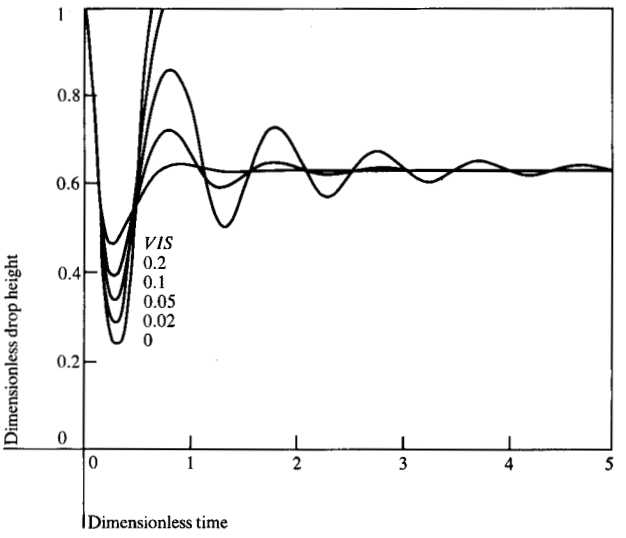

Figure 9 Drop height *vs* time during contact (for various *VIS* with $ST = 0$ and $W = 4$).

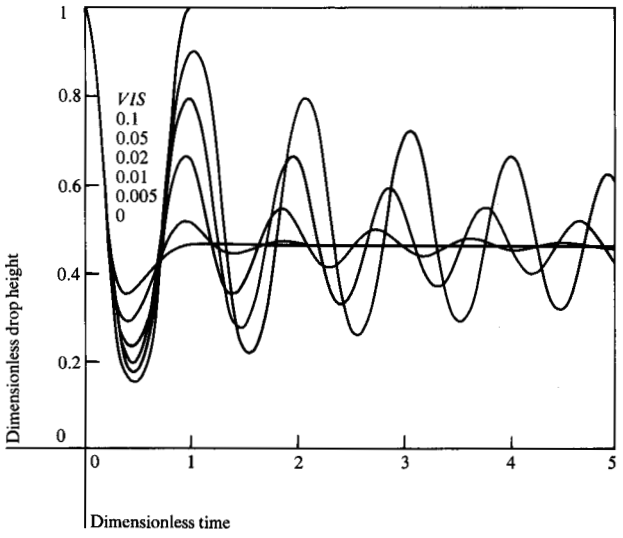

Figure 10 Drop height *vs* time during contact (for various *VIS* with $ST = -0.5$ and $W = 4$).

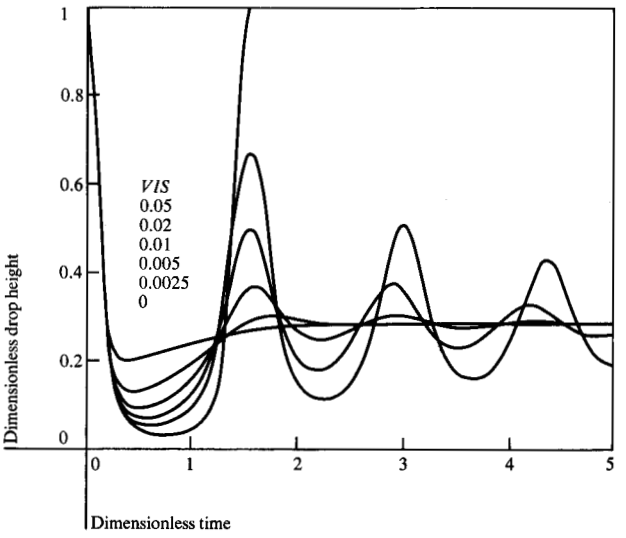

Figure 11 Drop height *vs* time during contact (for various *VIS* with $ST = -0.866$ and $W = 4$).

the inviscid value $VIS = 0$ to a value that represents a highly damped case. In these curves t^* ranges from 0 to 5 whereas in Fig. 2 it ranges from 0 to 2 and in Figs. 3 and 4 it ranges from 0 to 1.5. Correspondingly, the Δt^* used in the numerical integration was 0.05 for Figs. 6–14, 0.02 for Fig. 2, and 0.01 for Figs. 3, 4, and 5. The convergence was checked in all cases by making test calculations with a smaller value of Δt^*. The figures were drawn with a digital plotter using a graphics software package that gives straight lines between the neighboring data points. This explains the straight line segments in the curves of Figs. 6–14.

Figures 6–8 show that when $VIS = 0$ the drop rebounds from the target surface, but if *VIS* is large enough, the drop remains on the surface and the x *vs* t^* curves somewhat resemble a damped single degree-of-freedom linear oscillator. In Fig. 6, where $ST = 0$, the drop

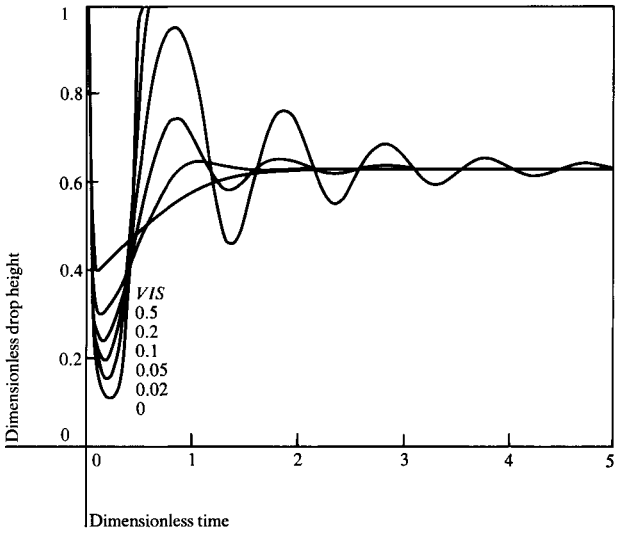

Figure 12 Drop height *vs* time during contact (for various *VIS* with $ST = 0$ and $W = 49$).

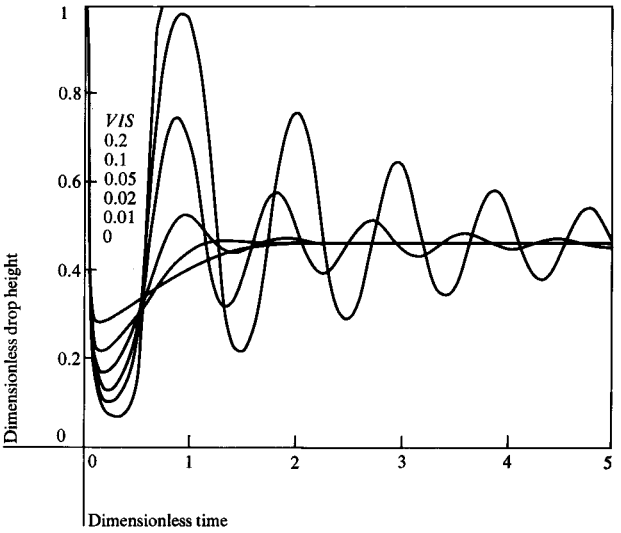

Figure 13 Drop height *vs* time during contact (for various *VIS* with $ST = -0.5$ and $W = 49$).

remains on the target surface for $VIS > 0.01$. As indicated in Figs. 7 and 8, a smaller value of *VIS* is required to prevent bounce-off for smaller values of *ST*. Also in Fig. 6 we see that for $VIS = 0.1$ the static condition is reached after two or three oscillations. This static drop height value $\bar{x}$ depends only on *ST* according to (27). Figures 7 and 8 show that the damping for $VIS = 0.1$ is more severe for the smaller values of *ST*. Figure 8 illustrates the nonsinusoidal nature of the drop height oscillation, and it also shows that the period depends on the damping parameter *VIS*. The curve for $VIS = 0.1$ does not oscillate; the drop height in this case monotonically decreases to its static value.

Figures 9–11 present a sequence similar to Figs. 8–10 except that *W* equals 4 rather than 1. Figures 12–14 present a similar sequence for *W* equals 49. Qualitatively the results are similar to those in Figs. 8–10, and they need not be discussed in detail.

Estimate for the viscosity parameter *C*

The viscosity parameter *C* introduced in (17) with units of inverse length can be estimated in terms of an unsteady boundary layer thickness. In Batchelor [7, p. 355] the frictional stress at an oscillating boundary is given by the real part of $\mu(1 + i)(U/\delta) \exp(int)$, where δ is the boundary layer thickness given by

$$\delta = \left(\frac{2\mu}{\rho n}\right)^{1/2} \tag{29}$$

and n is the angular frequency,

$$n = 2\pi f = 2\pi/T. \tag{30}$$

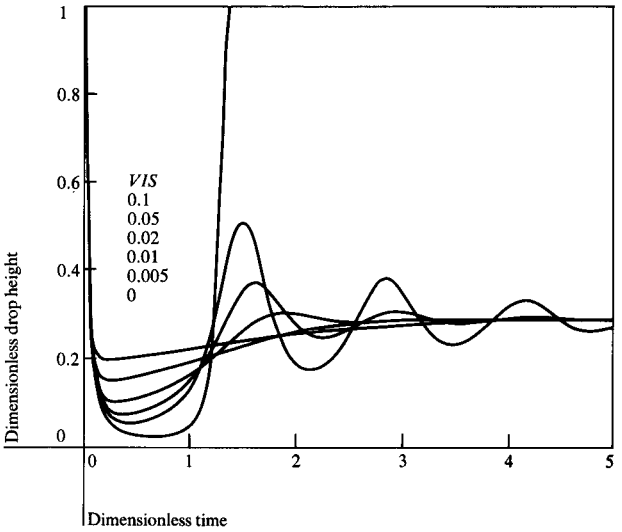

Figure 14 Drop height *vs* time during contact (for various *VIS* with $ST = -0.866$ and $W = 49$).

For our application we take *T* to be the period observed in the numerical results which, in view of (22), is of the order

$$T = (\rho a^3/\sigma)^{1/2}. \tag{31}$$

Then *C* in (17) is given by

$$C = \delta^{-1}, \tag{32}$$

where

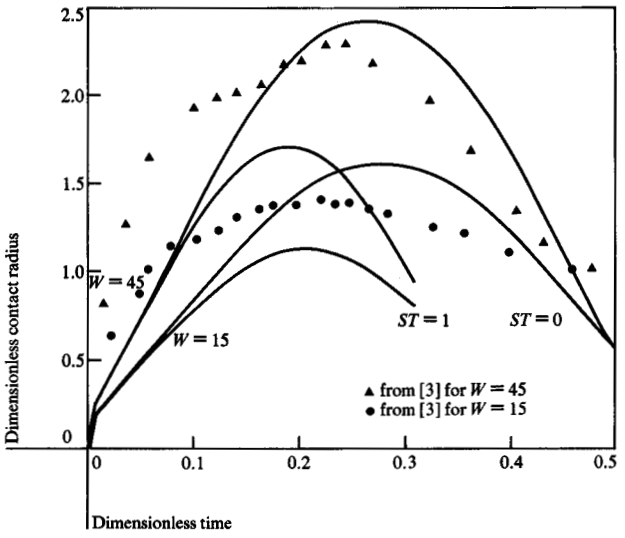

Figure 15 Contact radius *vs* time during contact (for $VIS = 0$; $ST = 0, 1$; and $W = 15, 45$—theory and experiment).

$$\frac{\delta}{a} = \left(\frac{\mu^2}{\pi^2 \rho \sigma a}\right)^{1/4}, \tag{33}$$

and, in view of (22) and the definitions of W and R, it follows that

$$VIS = \frac{\sqrt{\pi}}{12}\left(\frac{W^{1/2}}{R}\right)^{1/2} = \frac{\sqrt{\pi}}{12}\left(\frac{\mu^2}{\rho a \sigma}\right)^{1/4}. \tag{34}$$

For ink-jet applications this expression is typically of order 0.1, which represents a fairly high value of damping in the numerical results presented in Figs. 6–14.

Comparison with experiments

There have been only a few experimental investigations of liquid drop impact on rigid surfaces, and these usually were for hot surfaces in heat transfer experiments. Wachters and Westerling [3] made photographs of drops impacting a polished gold surface maintained at a temperature of 400°C. Their Fig. 12 shows contact surface radius as a function of a dimensionless time after impact for three different impact velocities. Their photographs (presented in their Figs. 9–11) show that a truncated sphere is close to the actual shape during the height reduction stage but not during the rebound stage. Since the temperature of their target surface is much greater than the boiling point of the liquid (water), the surface is not wetted, and the surface tension on the contact surface should be that appropriate to water in steam at the boiling point. The droplets were discharged at an initial temperature of 99°C so ρ and σ on the free surface were taken as the boiling point values. Evidently, though never specifically stated, they used $\rho/\sigma = 1.612\ s^2/m^3$. This gives W equal to 15, 45, and 183 for the three velocities used in their Fig. 12. Since the value 183 is much higher than their observed critical value for splatter, only their 15 and 45 values of W are useful for comparison with our analytical results. Figure 15 shows dimensionless contact radius λ_b/a *versus* dimensionless time t^* for $W = 15$, 45 and for $ST = 0$, 1 with $VIS = 0$. These results were calculated with use of (2) after x *versus* t^* had been obtained for these parameters. Also shown on Fig. 15 are the experimental results from Fig. 12 of Wachters and Westerling [3]. It is clear from these results that the $ST = 0$ curves correspond more closely to experiment than do the $ST = 1$ curves. It is expected that the surface tension next to the 400°C surface would be less than the value in air, so that ST would be less than unity. We also observe that the experimental curves for contact radius increase faster and approach zero slower than do the theoretical results. The latter discrepancy is understandable if we observe that upon rebound the experimental drops become quite elongated rather than retaining the shape of a truncated sphere.

It is possibly more useful for applications to display the minimum drop height and maximum contact radius as a function of Weber number. This occurs when dx/dt vanishes, and hence at the first minimum in Figs. 2–14. When $VIS = 0$, we can use conservation of energy to derive the necessary condition for this minimum. Since from (11) KE vanishes with dx/dt, we get

$$KE^0 + PE^0 = PE,$$

or with use of (6) and (13)–(15), x_{min} satisfies

$$(2 - ST)\,x^3 - \frac{3}{2}\left(\frac{W}{6} + 2\right)x + (1 + ST) = 0.$$

After this cubic is solved for x_{min}, the maximum contact radius is computed from the result and the second of (2). Figures 16(a) and (b) show x_{min} and $(\lambda_b/a)_{max}$ *versus* $(W/6) + 2$ for various values of ST. The experimental results for $W = 15$, 45 from [3] are shown in Fig. 16(b), again indicating close agreement with the calculated result for $ST = 0$.

Summary

A truncated sphere model is used with Lagrangian methods to study analytically the impact of a spherical drop against a flat rigid surface. The method is similar to that used by Kendall and Rohsenow [6] but differs from theirs in three ways. First, our kinetic energy expression is different. We use (7) with an assumed flow field for axisymmetric stagnation flow (8) to calculate KE. In [6] a form was used that was similar to one obtained for the cylindrical drop model, but with two constants subse-

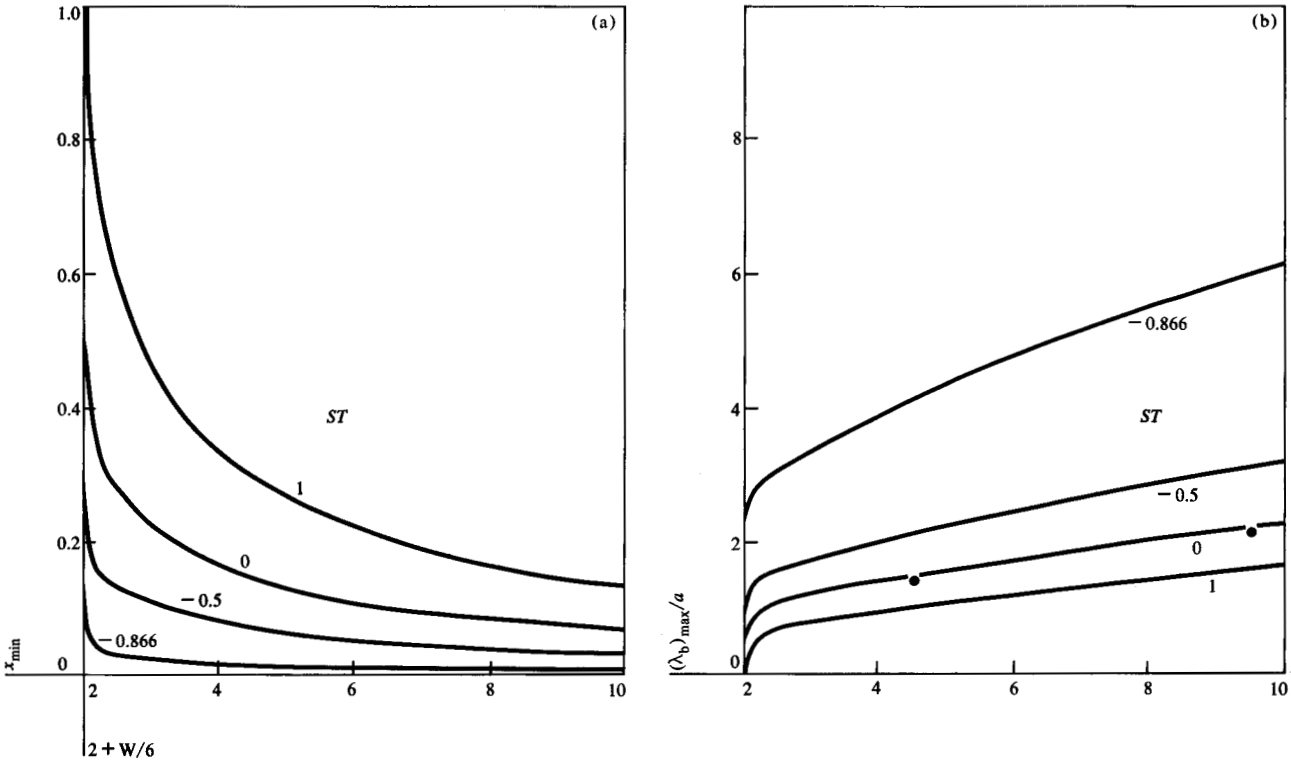

Figure 16 Dependence of minimum height and maximum contact radius on 2 + *W*/6.

quently determined by comparing results for free vibration of the drop. Second, we allow different arbitrary values of free surface tension and contact surface tension, whereas in [6] the latter was set equal to zero. Third, we introduce dissipation into our model.

The analysis predicts a plausible drop impact dependence on three parameters *W*, *ST*, and *VIS*, which represent the impact drop Weber number, the ratio of surface tensions, and the viscosity parameter. Comparison with a limited set of experiments indicates that the analytical results should be useful in predicting spot size in ink jet printing.

Additional experimental results would be helpful in determining the appropriate values for the viscosity parameter.

Acknowledgment

The authors gratefully acknowledge helpful discussions of S.E.B. with Professor Gail McCarthy (formerly Gail Kendall, coauthor of [6]). We also wish to thank Dr. F. C. Lee for his discussions and especially for his suggestion that the unsteady boundary layer be used for estimating the viscosity parameter *C*.

References

1. M. Cantow and L. Nebenzahl, IBM General Products Division, San Jose, private communication.
2. O. G. Engel, "Waterdrop Collisions with Solid Surfaces," *J. Res. Nat. Bureau of Standards* **54,** 281–298 (1955).
3. L. H. J. Wachters and N. A. J. Westerling, "The heat transfer from a hot wall to impinging water drops in the spherical state," *Chem. Eng. Sci.* **21,** 1047–1056 (1966).
4. C. O. Pederson, "An Experimental Study of the Dynamic Behavior and Heat Transfer Characteristics of Water Droplets Impinging upon a Heated Surface," *Int. J. Heat and Mass Transfer* **13,** 369–381 (1970).
5. M. A. Styricovich, Yu. V. Baryshev, G. V. Tokiklauri, and M. E. Grigorieva, "The Mechanism of Heat and Mass Transfer Between a Water Drop and a Heated Surface," Paper PB-22, presented at the Sixth International Heat Transfer Conference, Toronto, Vol. 1, 239–243, 1978.
6. G. E. Kendall and W. M. Rohsenow, "Heat Transfer to Dispersed Flows and Sprays: The Liquid Contribution," *Proceedings of 2nd International Multiphase Flow and Heat Transfer Symposium*, Miami, FL, 1979.
7. G. K. Batchelor, *An Introduction to Fluid Dynamics*, Cambridge University Press, Cambridge, England, 1970.

Received March 23, 1981; revised May 21, 1981

S. E. Bechtel and D. B. Bogy are in the Department of Mechanical Engineering, University of California, Berkeley, California 94720; F. E. Talke is located at the IBM Research Division laboratory, 5600 Cottle Road, San Jose, California 95193.